

DUAL BEAM OPTICAL COHERENCE TOMOGRAPHY: SIGNAL IDENTIFICATION FOR OPHTHALMOLOGIC DIAGNOSIS

Wolfgang Drexler,[†] Oliver Findl,[‡] Rupert Menapace,[‡] Andreas Kruger,[‡] Andreas Wedrich,[‡] Georg Rainer,[‡] Angela Baumgartner,[†] Christoph K. Hitzenberger,[†] and Adolf F. Fercher[†]

[†]University of Vienna, Institute of Medical Physics, Währinger Straße 13, A-1090 Vienna, Austria;

[‡]General Hospital of Vienna, Department of Ophthalmology, Währinger Straße 18-20, A-1090 Vienna, Austria

(Paper JBO/IB-012 received Aug. 21, 1997; revised manuscript received Nov. 11, 1997; accepted for publication Nov. 12, 1997.)

ABSTRACT

The dual beam version of optical coherence tomography can be used for noninvasive, high-resolution imaging of the human eye fundus, enabling *in vivo* visualization of retinal morphology as well as accurate quantification of the thickness profiles of its layers. Interferometric fundus signals—optical A-scans—and retinal tomograms of patients with glaucoma, diabetic retinopathy, and age-related macular degeneration are compared with those of healthy, normal subjects to elucidate the origin of the signal peaks detected and to investigate and interpret the retinal microstructures contained in the cross-sectional images. © 1998 Society of Photo-Optical Instrumentation Engineers. [S1083-3668(98)01701-8]

Keywords optical coherence tomography; partial coherence interferometry; glaucoma; diabetic retinopathy; age-related macular degeneration.

1 INTRODUCTION

In the past decade there have been tremendous efforts toward the development of novel noninvasive techniques for ophthalmologic diagnosis that are capable of imaging the retina, providing new insights into its microstructural morphology, and yielding quantitative information about the contour and the thickness profile of its layers. Clarification of fundamental questions about this highly sensitive organ, much earlier diagnosis, and an objective monitoring of several ocular diseases, as well as a more accurate evaluation of the efficiency of current therapeutic ophthalmologic treatments should be the consequence of these efforts.

A special confocal scanning laser ophthalmoscope (SLO), the Heidelberg retina tomograph (HRT; Heidelberg Engineering Optische Meßsysteme GmbH, Heidelberg, Germany) provides fast three-dimensional topographic measurements of the optic disk by raster scanning the retina.^{1,2} Morphometric changes expressed by several topographic parameters can be quantified for glaucoma diagnosis. Besides excavation contour changes of the optic disk, glaucomatous damage also results in loss of retinal ganglion cells, with a thinning of the retinal nerve fiber layer, the innermost retinal layer. Glaucoma patients have local-

ized defects in the retinal nerve fiber layer, with a corresponding functional abnormality that may precede the onset of glaucomatous field loss by up to 6 years.³ Therefore, quantitative measurements of the distribution of the retinal nerve fiber layer thickness (RNFLT) in the region of the optic disk would help to discriminate glaucoma suspects from normal persons at a much earlier stage.

A promising approach for an objective quantification of the RNFLT is the new clinical model of the nerve fiber analyzer (LDT Inc., San Diego, California).^{4,5} This special version of SLO uses the birefringent properties of the retinal layer to accurately and rapidly measure its thickness. It uses a normative database—a collection of hundreds of two-dimensional RNFLT distribution maps obtained from healthy subjects in a multicenter study—for easy identification and management of glaucoma patients with 96% sensitivity and 93% specificity.^{6,7}

The measurement of retinal thickness, which is especially important for diagnosis and monitoring of diabetic retinopathy as well as macular holes, can be performed noninvasively and very quickly with an extension of the slit-lamp biomicroscopy technique, the retinal thickness analyzer.^{8,9} This technique has also recently been reported to be in use in clinical studies.¹⁰

Address all correspondence to Wolfgang Drexler. Tel: 431 40480333; Fax: 431 4024030; E-mail: wolfgang.drexler@univie.ac.at

1083-3668/98/\$10.00 © 1998 SPIE

A completely different approach to visualizing retinal microstructures and to obtaining quantitative data on its layers is accomplished by a noninvasive optical ranging technique called optical coherence tomography (OCT).^{11,12} It is based on the optical coherence-domain reflectometry principle and uses a special interferometric technique, partial coherence interferometry, employing partially coherent light beams for optical ranging.¹³⁻¹⁵ Two related versions of this technique have been developed in the past.

The first uses a classical interferometric setup,¹⁶ which is rather sensitive to longitudinal eye movements during measurement. High-resolution images of the human eye fundus can be obtained rapidly, and several clinical studies have been performed.¹⁷⁻¹⁹ This version of OCT has now advanced to a powerful imaging technology that is also used in other medical fields because of its ability to provide optical biopsy.^{20,21}

The second is a special dual beam version of this interferometric technique,^{13,22} which eliminates any influence of longitudinal eye motion during measurement by using the cornea as a reference surface; this enables (sub)micrometer precision biometry of the human eye *in vivo*. Depending on the intraocular distance to be measured, precisions from 0.3 to 10 μm can be achieved.²³⁻²⁶ In addition, cross-sectional retinal images and precise quantification of thickness profiles of several retinal and choroidal layers can be obtained.²⁷⁻²⁹ This dual beam version of OCT has now been used in a clinical setting for the first time and its clinical feasibility has been investigated in several studies.³⁰ In this study, selected pathologic cases were investigated. The interferometric signals and tomograms obtained are compared with those of normal eyes to determine the origin of the interferometric signal peaks and to interpret the retinal microstructures revealed by the tomograms.

2 METHODS

2.1 DUAL BEAM OPTICAL COHERENCE TOMOGRAPHY

The principle of the dual beam version of OCT was described in detail in previous papers.^{13,22,28} Distances to different points of the retina are measured along linear or circular scans across the human eye fundus *in vivo*. The coherence properties of light are used to obtain the longitudinal positions of light-reflecting sites within the eye. So-called optical A-scans are recorded and then plotted to form topographic as well as cross-sectional tomographic images containing quantitative information about the contour, the thickness profile, and the microstructure of different retinal layers.^{27,28} These tomograms are synthesized by converting the intensity values of the optical A-scans into color or gray-scale values according to a logarithmic or linear scale,

and by mounting them to form a two-dimensional (B-scan) cross-sectional image. In this work the same logarithmic scale was used for all tomograms to convert the amplitude of the A-scans into pixel colors.

The most recent version of the dual beam OCT uses an infrared superluminescent diode (SLD) (SLD C86142E, EG&G Optoelectronics, Canada) with a center wavelength of $\lambda_1 \approx 855 \text{ nm}$, a spectral bandwidth of 24.6 nm (full-width at half-maximum), yielding a longitudinal resolution of about 15 μm in air, i.e., about 10 μm in ocular media (after dividing it by the group refractive index of the respective ocular media). In air, the axial resolution is inversely proportional to the spectral bandwidth of the light source used;³¹ in the dispersive ocular media, it depends on the group dispersion and the path length.^{32,33}

Since all the distances obtained by OCT are optical distances, they have to be divided by the group refractive index³⁴ of the respective eye medium of 855 nm wavelength to obtain the geometrical distances.²² In the conversion of the optical to geometrical thickness, a group refractive index of $n_g = 1.4$ for the retinal layers was assumed (no measured value of n_g at $\lambda \approx 855 \text{ nm}$ is reported for these layers in the literature). The mean group refractive index of the lens is about 1.4065, and that of the vitreous humor is approximately 1.3440 for $\lambda = 855 \text{ nm}$.³² It is assumed that the group refractive index of the retinal layers is slightly higher than that of the vitreous, but not higher than that of the lens. Using $n_g = 1.35$ instead of 1.4 would cause a difference in length measurement of 3.6%. On the other hand, errors in the refractive index can be neglected if only optical thickness values are used for comparing the thickness of the retinal layers of healthy and disordered retinas.

2.2 PATIENTS AND *IN VIVO* MEASUREMENTS

All research and measurements performed in this study followed the tenets of the Helsinki agreement; informed consent was obtained from all subjects after the nature and possible consequences of the study had been explained. The study was approved by the ethics committee of the Vienna University School of Medicine.

In addition to the OCT measurements, patients underwent a complete ophthalmologic examination, including medical and family history, visual acuity testing, measurement of intraocular pressure using applanation tonometry, slit-lamp examination of the ocular media, and funduscopy. Humphrey 30-2 visual field testing and HRT imaging was performed in glaucoma patients; fluorescein angiogram photos were taken from patients with diabetic retinopathy; and SLO images (SLO 101, G. Rodenstock GmbH, Heidelberg) were obtained from patients with age-related macular degenera-

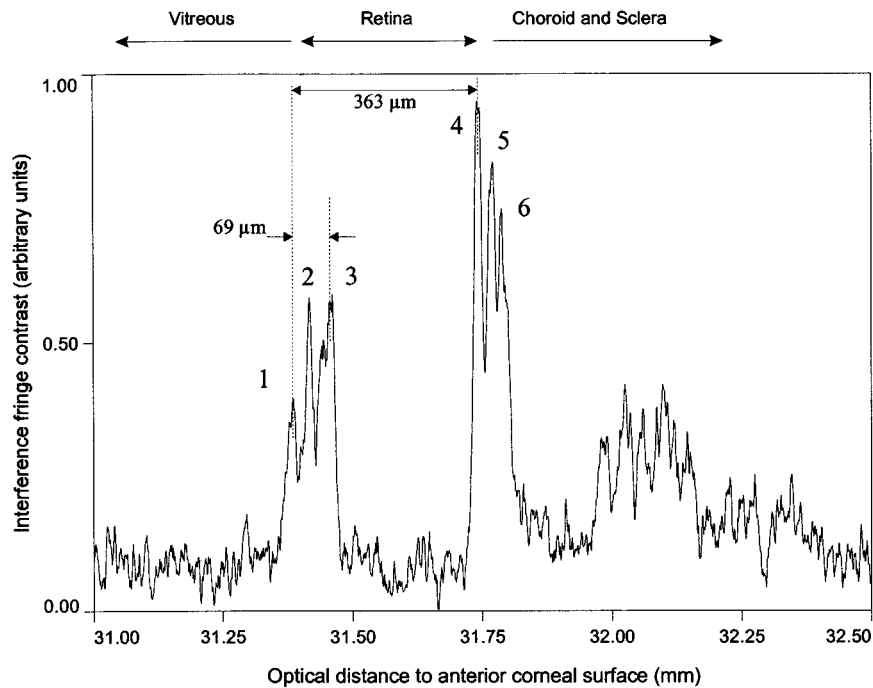


Fig. 1 Longitudinal scan (optical A-scan) of a normal human eye near the optic disk at a horizontal angle to the vision axis of 10 deg nasal. Several peaks from different retinal and choroidal structures can be observed. The optical retinal nerve fiber layer thickness (distance between peaks 1 and 3) as well as the optical retinal thickness (distance between peaks 1 and 4) are indicated.

tion to document the fundus region investigated by OCT.

During *in vivo* measurements of the human eye, laser safety regulations have to be followed. An intensity of about $220 \mu\text{W}$ or $572 \mu\text{W}/\text{cm}^2$ (averaged over a 7-mm aperture) was applied during measurement. In the human eye, this intensity is permitted for about 28 min.³⁵ A single measurement on the fundus—a longitudinal scan over 3 mm—performed in this study lasts 0.5 s. Four to eight single longitudinal scans at each of the positions on the fundus were used to synthesize tomograms along linear or circular scans. The maximum time of continuous illumination was about 30 s (for four longitudinal scans over 1.5 mm at each measurement position). This is far below safety limits. No anesthesia of the eye and no mydriatics for pupil dilation are needed for *in vivo* measurements.

3 RESULTS AND DISCUSSION

Figure 1 shows a typical example of an optical length measurement, a so-called optical A-scan, of a normal human eye *in vivo* that was obtained near the optic disk at a scanning angle of 10 deg nasal to the vision axis. This longitudinal scan (averaged over ten measurements) was performed over a distance of 1.5 mm, ranging from 31 to 32.5 mm (with the cornea as the reference surface). It took about 0.25 s. Several peaks from different retinal and choroidal microstructural layers can be distinguished. Peaks 1 to 3 seem to be generated by inner retinal layers that are close to the vitreous. There is evi-

dence that peak 1 originates from light reflected at the internal limiting membrane, which is closest to the vitreous. Peak 3 probably originates from the posterior surface of the retinal nerve fiber layer, giving rise to the assumption that the distance between these two peaks corresponds to the optical retinal nerve fiber layer thickness. In Figure 1, the thickness of this layer is about $69 \mu\text{m}$, yielding a geometrical thickness of about $49 \mu\text{m}$ by dividing the optical thickness by the group refractive index n_g of the retina (assuming $n_g=1.4$).

The exact origin of peak 2 is not quite clear at present. Sometimes only two peaks (peaks 1 and 2 in Figure 1) are detected. The distance between these two is then used to determine the thickness of the retinal nerve fiber layer. Peak 4 probably originates from the retinal pigment epithelium. The distance to peak 1 is equal to the optical retinal thickness, in this case $363 \mu\text{m}$, yielding a $259\text{-}\mu\text{m}$ geometrical retinal thickness (assuming $n_g=1.4$). In normal subjects, peaks 5 and 6 probably arise from light reflected at choroidal layers. In patients with age-related macular degeneration (AMD) with soft drusen, the distance between peaks 4 and 5 might indicate the thickened Bruch's membrane (see Figure 8 in Sec. 3.3.1). The precision with which the retinal interfaces can be located, is about 3 to $4 \mu\text{m}$ (standard deviation of multiple recorded consecutive measurements of the optical distance between the cornea and the retinal interface). Dividing this value by the mean group refractive index $n_g=1.35$ of the eye media²² yields a geometric precision of

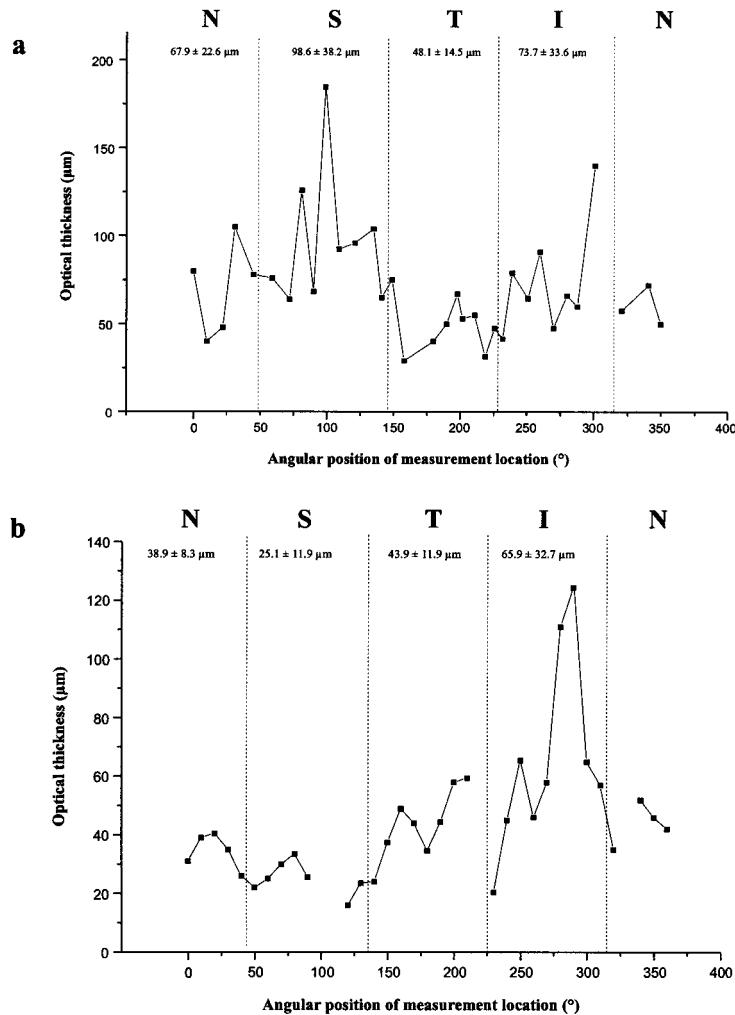


Fig. 2 Circumpapillary distribution of the optical retinal nerve fiber layer thickness around the rim of the optic disk along a circle with approximately 2.3 mm diameter of a normal (a) and a glaucomatous (b) human eye. Significant RNFLT “humps” in the superior and inferior quadrants can be observed in the normal human eye. The lack of a “hump” in the RNFLT contour of the superior quadrant is correlated to the inferior nasal visual field loss in the glaucomatous eye (see Figure 4). The mean value \pm variability of the optical nerve fiber layer thickness for each quadrant is indicated.

about 2 to 3 μm (the precision to which the geometric distance of the corneal–retinal interface can be determined). The exact origin of some of these peaks indicated in Figure 1 is not quite clear yet. Therefore special pathologic cases were investigated and the interferometric signals compared with those obtained in normal eyes.

3.1 GLAUCOMA

To explain the origin of peaks 1 and 3, indicated in Figure 1, which enable the measurement of the optical RNFLT, the papillary region of normal and glaucomatous eyes was measured, since blindness ensues from gradual loss of optic nerve fibers and therefore there is a thinning of the RNFLT in this ocular disease.³⁶

Figure 2 shows the circumpapillary distribution of the optical retinal nerve fiber layer thickness (i.e., the distance between peaks 1 and 3, of Figure 1) in

a normal (a) and glaucomatous (b) eye along a circle approximately 2.3 mm diameter, around the rim of the optic disk. Thirty-six measurements were obtained at polar angle increments of 10 deg. The area around the optic disk was divided into four quadrants: temporal (T), nasal (N), inferior (I), and superior (S). The borders of these four quadrants are also indicated. Figures 3 and 4 show the Humphrey 30-2 visual fields and the topographic maps of the optic disk obtained by an HRT of the corresponding normal [see Figure 2(a)] and glaucomatous [Figure 2(b)] eye. Three 10 \times 10-deg measurements of the optic disk were obtained with the HRT and automatically averaged. Whereas the visual field of the healthy eye of a 27-year-old subject is normal and the HRT topographic map of the optic disk shows normal cupping (Figure 3), a diffuse increase in threshold (mean deviation -8 dB) and an absolute inferior nasal field defect in the visual field

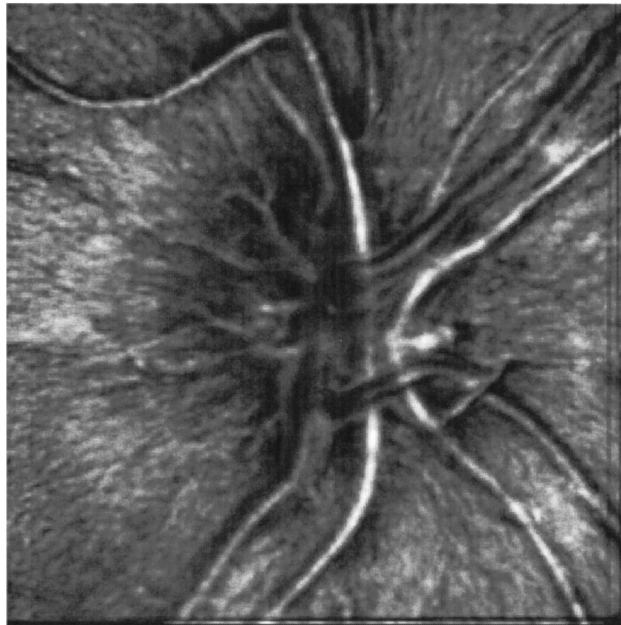
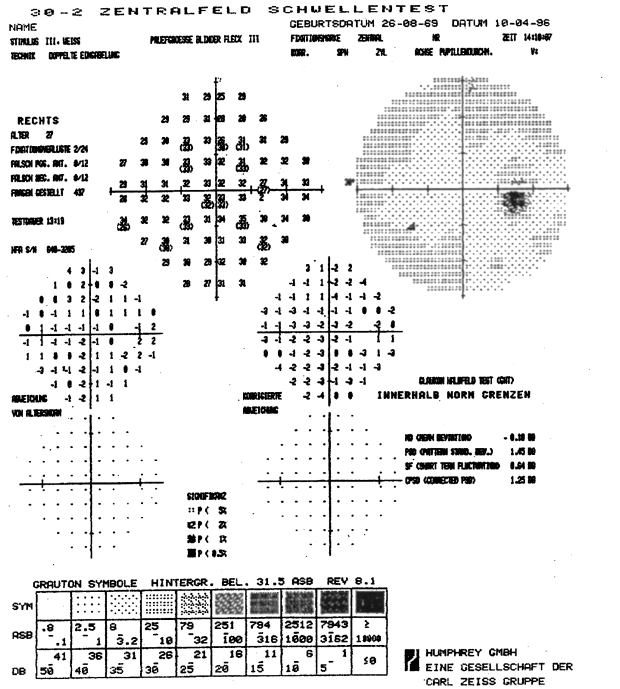


Fig. 3 Humphrey 30-2 visual field (left) and Heidelberg retina tomographic map (right) of a normal eye.

of the glaucomatous eye can be observed (Figure 4). The HRT topographic map of the optic disk reveals an enlarged cupping.

In the normal eye [Figure 2(a)], the optical RNFLT ranged from 30 to 190 μm (mean: 72 μm);

in this case it was 20 to 135 μm (mean: 52 μm) for the geometrical thickness of this layer. In the glaucomatous eye [Figure 2(b)], the optical RNFLT ranged only from 17 to 125 μm (mean: 44 μm), a geometrical thickness of 12 to 90 μm (mean: 31

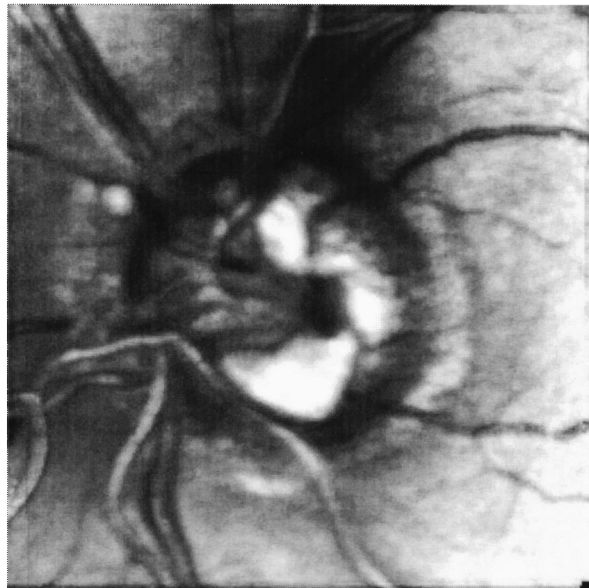
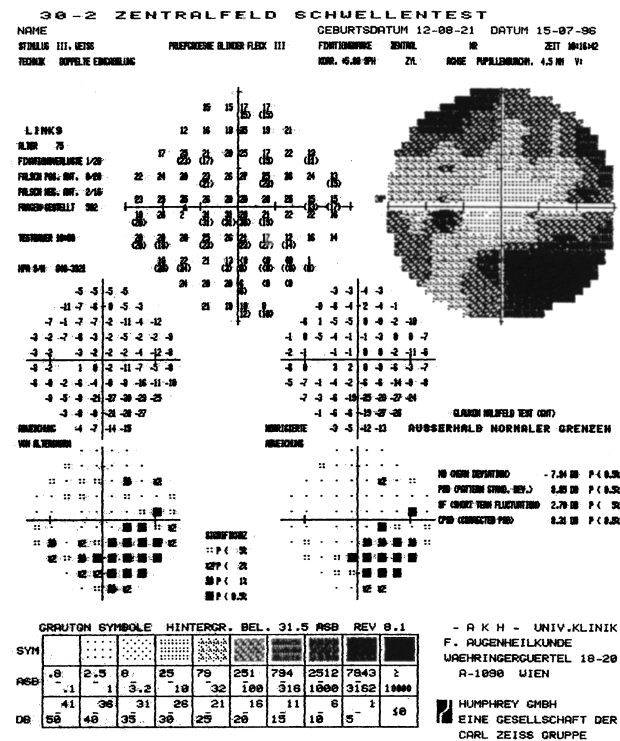


Fig. 4 Humphrey 30-2 visual field (left) and Heidelberg retina tomographic map (right) of a glaucomatous eye.

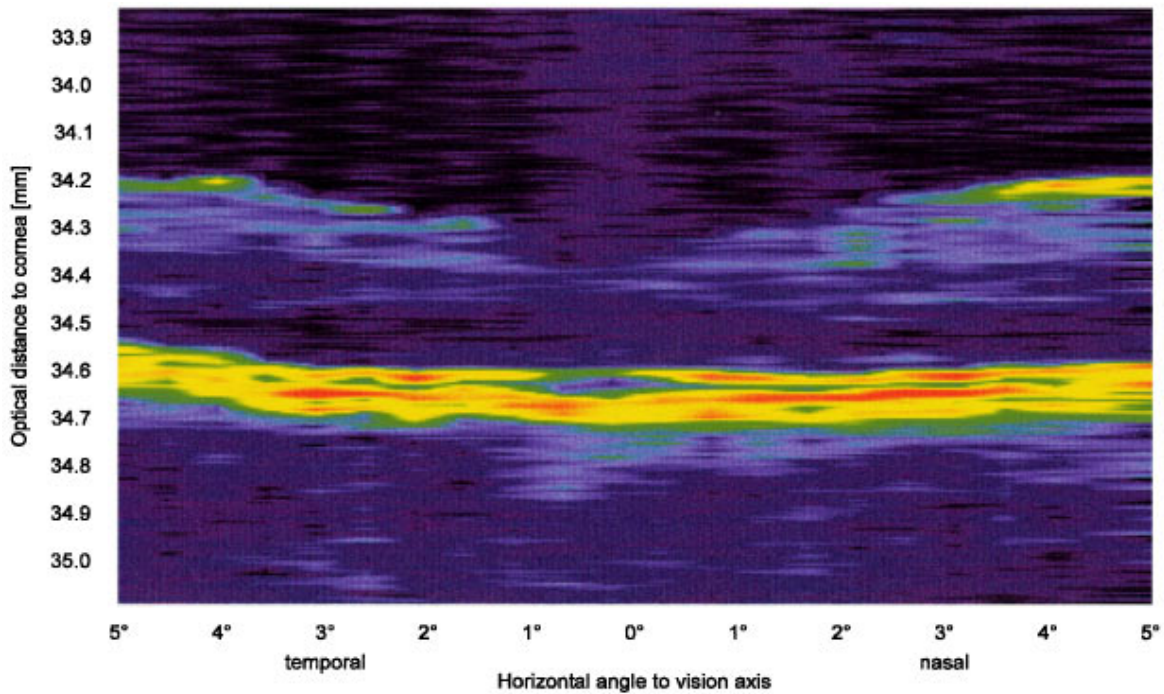


Fig. 5 Horizontal cross-sectional image (~ 3 mm transversal \times ~ 1.1 mm horizontal optical distance) of the fovea of a normal human subject (logarithmic color scale). The shape of the fovea, given by the contour of the internal limiting membrane, the contour of the retinal pigment epithelium, and subretinal structures such as choroidal layers can be observed. The corresponding retinal thickness is given in Table 1.

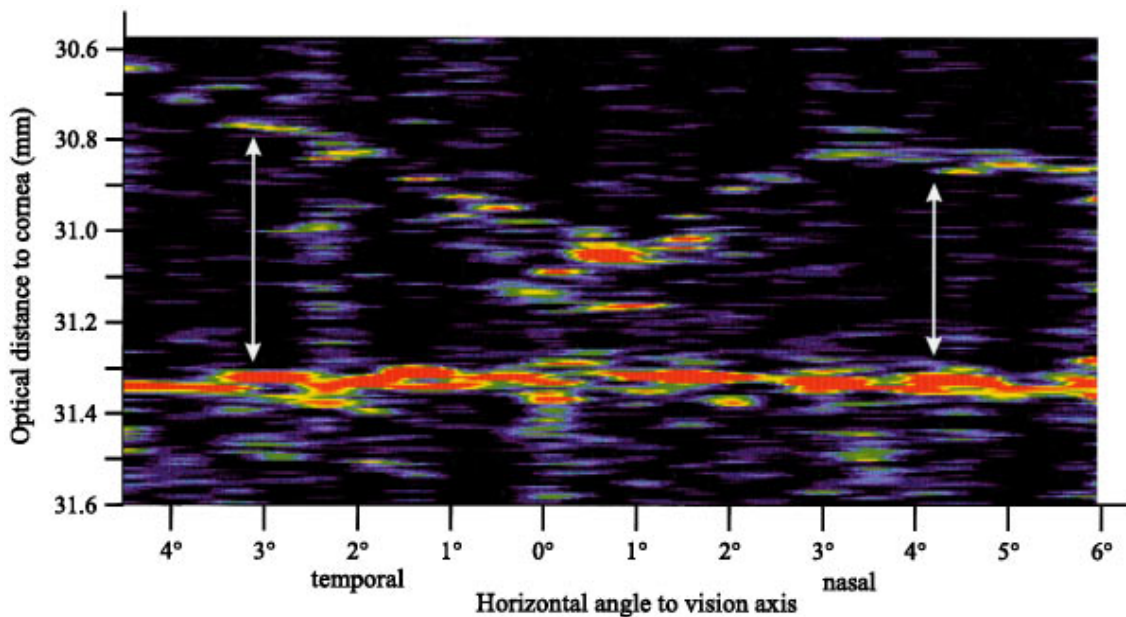


Fig. 6 Horizontal foveal cross-sectional tomogram of a patient with a macular edema (logarithmic color scale). The position of this scan is indicated in the fluorescein angiogram in Figure 7. A thickening due to the macular edema, especially in the temporal region, can be observed (indicated by arrows). For the respective retinal thicknesses, see Table 1.

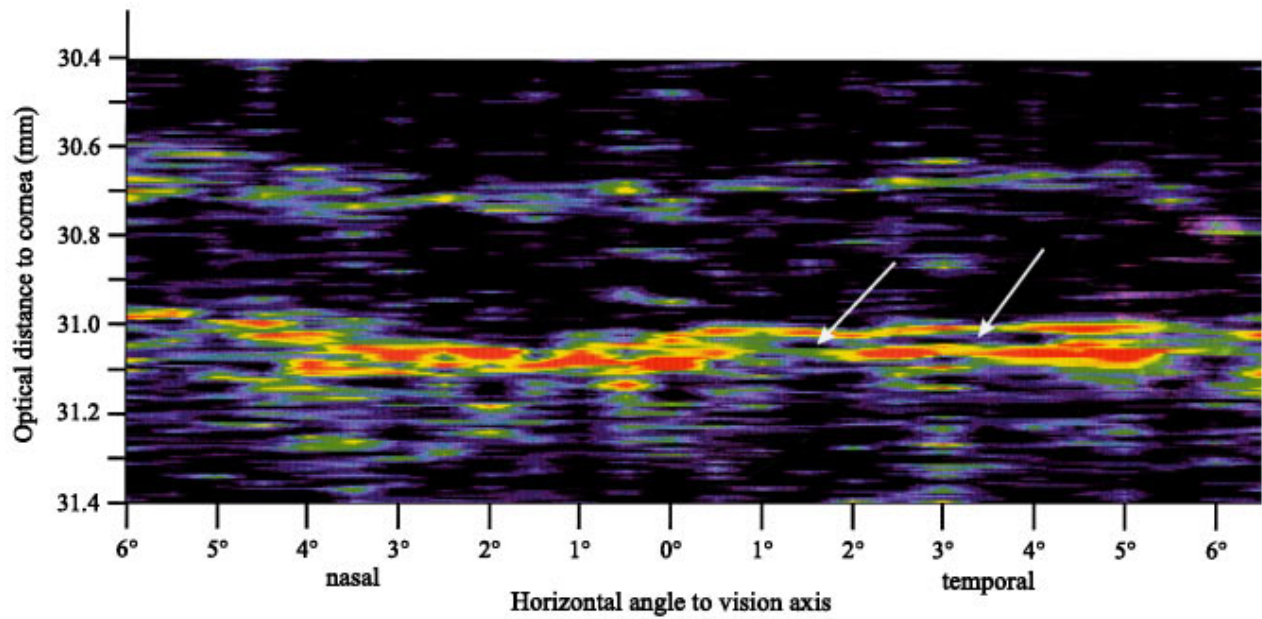


Fig. 8 Horizontal fundus tomogram of an AMD patient with soft drusen (logarithmic color scale). The location of the scan is indicated in Figure 9. A thickening of Bruch's membrane due to soft drusen can be clearly observed (indicated by the arrows). In the nasal region, a region with only a few drusen (Figure 9), no thickening of this layer can be observed (see Table 1).

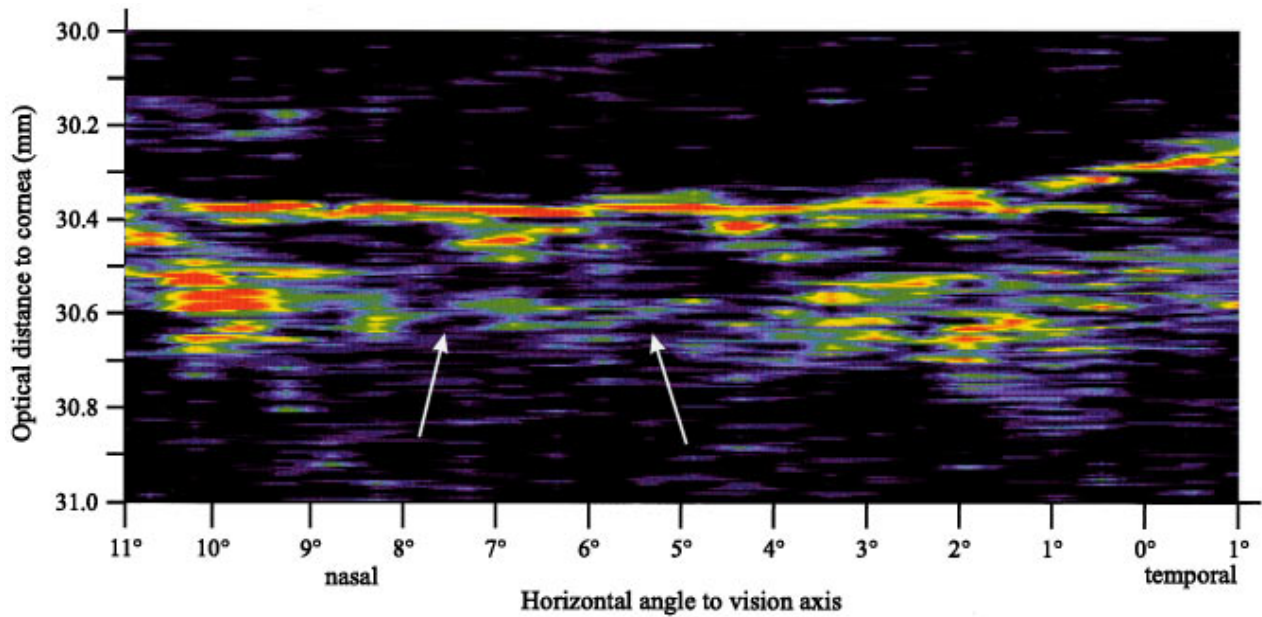


Fig. 10 Horizontal cross section of an AMD patient with areolar atrophy (logarithmic color scale). The location of the scan is indicated in Figure 11. Owing to the loss of the retinal pigment, the signal intensity has decreased and has become even weaker than that of signals reflected at the internal limiting membrane (peak 1 in Figure 1). In some areas, the signal reflected at the retinal pigment epithelium has nearly vanished (indicated by the white arrows in Figure 10). A thinning of the retina can be diagnosed and quantified (Table 1).

μm), respectively. Due to glaucomatous damage, the mean RNFLT of the glaucomatous eye is only about 60% of that measured in the normal eye. The mean RNFLT \pm variability for each quadrant is also indicated in both plots of Figure 2. In some cases, at 310 deg in the normal eye [Figure 2(a)] and at 220 and 340 deg in the glaucomatous eye [Figure 2(b)], no signal from the posterior surface of the retinal nerve fiber layer was detected, probably due to vessels, preventing the determination of the thickness of this layer. Significant thicknesses "humps" can be observed in the normal eye [Figure 2(a)], showing two distinct maxima ("double hump") of the retinal nerve fiber layer thickness, which coincide with the location of the superior and inferior arcuate bundles of the retinal nerve fiber layer.^{2,6,7,37-39} In the glaucomatous eye [Figure 2(b)], no "double hump configuration" of the circumpapillary distribution of the thickness of this layer can be observed. Only one "hump" of significant thickness could be detected in the inferior region. The lack of the thickness "hump" in the superior region correlates with the inferior nasal visual field loss detected by automated perimetry (Figure 4). At two positions, at 100 and 110 deg, only one peak corresponding to the internal limiting membrane could be detected. It seems that in this region, due to the severe nerve fiber layer defect (see the perimetry in Figure 3), the RNFLT is below the resolution (10 to 12 μm) of the instrument.

3.2 DIABETIC RETINOPATHY PATIENT

The optical retinal thickness can be measured from the distance given by peaks 1 to 4 in Figure 1. The intensities of longitudinal scans (Figure 1) at different angles between the vision axis and the measurement directions have been converted into pixel colors and mounted to synthesize a two-dimensional false color tomogram. Figure 5 (color plate) shows such a horizontal cross-sectional *in vivo* image in the region between 5 deg temporal and 5 deg nasal, resulting in an area of ~ 3 mm (transversal) \times ~ 1.1 mm (longitudinal) optical distance with a longitudinal resolution of ~ 10 μm and a transversal resolution of ~ 150 μm . The latter is limited by microsaccades of the human eye. The shape of the fovea, which is determined by the contour of the inner limiting membrane, the contour of the retinal pigment epithelium, and subretinal structures such as choroidal layers, can be observed. The distance between the inner limiting membrane and the retinal pigment epithelium (i.e., peaks 1 and 4 in Figure 1) is the (optical) retinal thickness. In Table 1 the mean (mean value over the whole scanned area), foveal (within a diameter of 1.5 mm), and parafoveal (nasal and temporal) geometrical retinal thicknesses are given.

In patients with diabetic retinopathy, a significant expansion of the extracellular space of the retina is observed, which is caused by the entry of plasma

Table 1 Geometrical retinal thickness obtained from the tomograms of different normal and pathologic cases (see the respective figures) with the mean value of the whole scanning area, foveal, and parafoveal regions (temporal and nasal) indicated.

Retinal thickness (μm)	Foveal (1.5 mm diameter)			Parafoveal (nasal)
	Mean	Parafoveal (temporal)	Parafoveal (nasal)	
Normal subject	231	207	257	273
Diabetic retinopathy patient	328	257	416	346
AMD-patient with soft drusen	238	242	222	247
AMD-patient with areolar atrophy	147	181	—*	131

* Linear scan was performed mainly in the nasal region (see Figures 10 and 11).

proteins due to leakage in the retinal perifoveal capillaries, resulting in a diffuse thickening of the retina,⁴⁰ so-called macular edema. A horizontal foveal cross-sectional tomogram of a patient with such an edema is shown in Figure 6 (color plate). Figure 7 shows a fluorescein angiogram in which the position of this scan (white line) as well as the position of the macular edema (arrow) in the temporal region are indicated. A thickening due to the macula edema, especially in the temporal region, can be observed in the tomogram in Figure 6 compared with that of a normal subject (Figure 5). The diffuse thickening of the posterior pole can also be quantified by measuring the (optical) retinal thick-

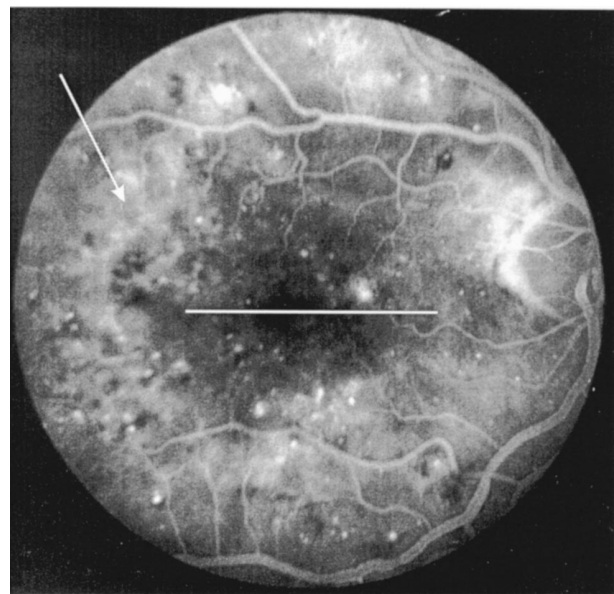


Fig. 7 Fluorescein angiogram of a patient with diabetic retinopathy, indicating the location of the scan shown in Figure 6 (white line) and the macular edema (white arrow).

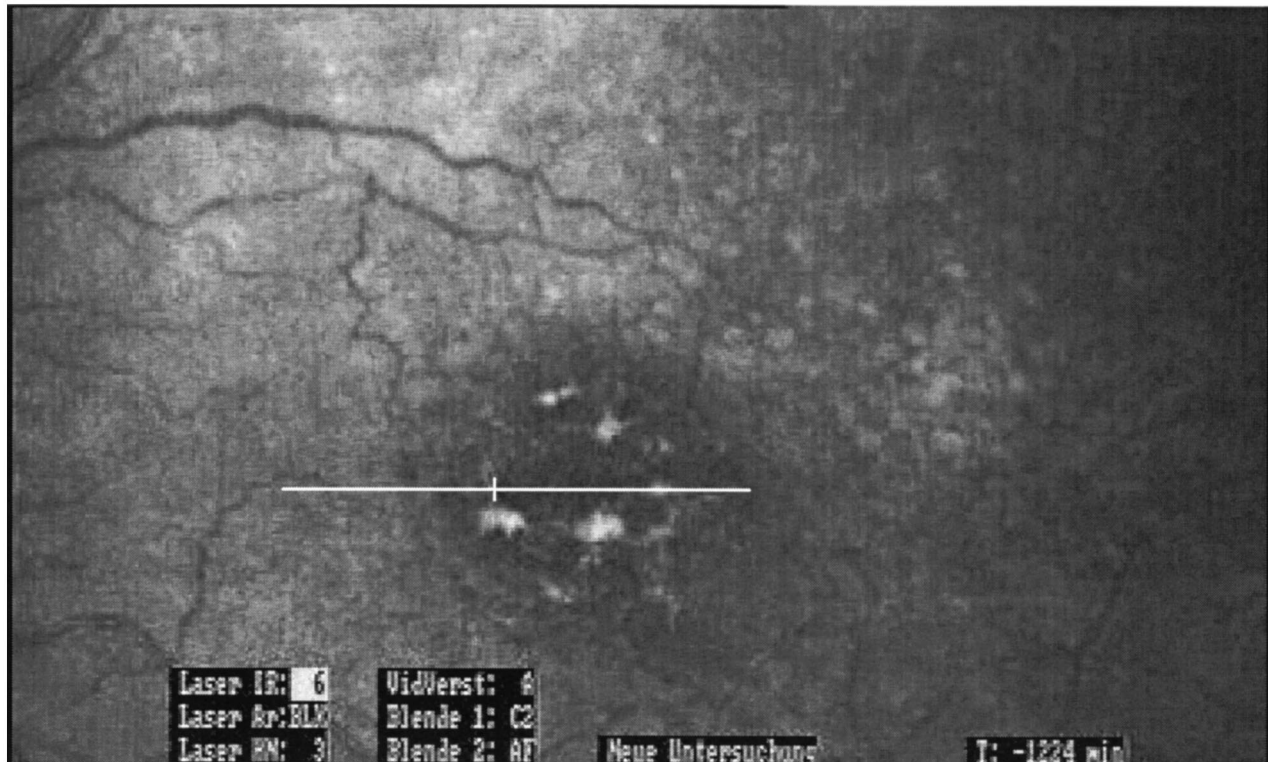


Fig. 9 Scanning laser ophthalmoscope image of an AMD patient with soft drusen. The location of the scan shown in Figure 8 is indicated as a white line. The cross-hair indicates the fixation point.

ness as the distance between peaks 1 and 4 (Figure 1). The measured (geometrical) values are given in Table 1. A thicker retina is measured in the case of the macular edema compared with the normal retina in all calculated regions.

3.3 AGE-RELATED MACULAR DEGENERATION

Age-related macular degeneration (AMD), alternatively termed age-related maculopathy (ARM), is the most common overall cause of blindness in the Western world. The clinical manifestation of AMD includes eccentrically located atrophic or exudative processes that decrease visual acuity if they spread onto the point of fixation, excessive numbers of soft and hard drusen, and pigmentary changes, which predispose to these complications. AMD is therefore based on diffuse morphologic changes at the level of the retinal pigment epithelium.

3.3.1 AMD with Soft Drusen

Drusen are yellowish deposits on the retinal pigment epithelium close to Bruch's membrane. At present they are classified as small (up to $124 \mu\text{m}$ diameter), round, and discrete (referred to as hard drusen), and generally larger ($>124 \mu\text{m}$; mostly $>250 \mu\text{m}$), with less sharp edge definition (referred to as soft drusen).³⁹

Figure 8 (color plate) shows a horizontal fundus tomogram of an AMD patient with soft drusen. The

location of the scan is depicted by the white line in the SLO image in Figure 9. The cross-hair indicates the point of fixation. In normal subjects, the distance between peaks 4, 5, and 6 (Figure 1) seems to indicate the thickness of choroidal layers. In AMD patients with soft drusen, the distance between peaks 4 and 5 probably indicates the thickening of Bruch's membrane due to soft drusen. This can be seen in the tomogram shown in Figure 8 (indicated by the arrows). In the nasal region, with only very few drusen (Figure 9), this phenomenon is not observed. A slight foveal thickening and a parafoveal thinning of the retina is detected in comparison with the normal subject (Table 1).

3.3.2 AMD With Areolar Atrophy

The more advanced forms of AMD are divided into a nonexudative or dry type, and an exudative-neovascular or wet form. In the dry form, the gradual disappearance of the retinal pigment epithelium results in a circumscribed area of atrophy that is often referred to as "geographic atrophy." The affected areas have no visual function, since loss of the retinal pigment epithelium is associated with fallout of photoreceptors as well as with a variable degree of choroidal atrophy.³⁹

Figure 10 (color plate) shows a horizontal cross-sectional tomogram at the nasal region of an AMD patient with such an atrophy. The affected, atrophied areas can clearly be seen as white areas in the

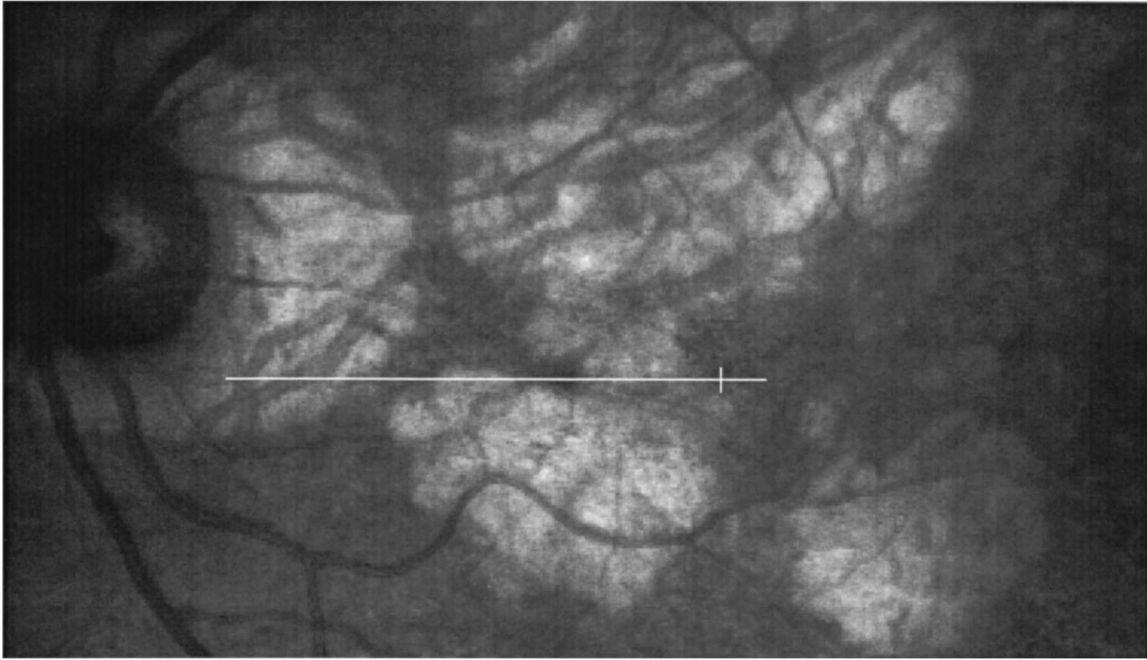


Fig. 11 Scanning laser ophthalmoscope image of an AMD patient with areolar atrophy. The location of the scan shown in Figure 10 is indicated by a white line. The cross-hair indicates the fixation point. White areas in the SLO image indicate scleral reflections due to the loss of the retinal pigment epithelium and choroidal atrophy.

SLO image of Figure 11. In these areas, scleral reflections due to the loss of retinal pigment can be observed. The white line in Figure 11 indicates the location of the OCT scan. The cross-hair indicates the point of fixation. Normally, the signals reflected at the retinal pigment epithelium are those of highest intensity (see Figures 1, 5, 6 and 8). Owing to the loss of pigment, however, the intensity of the signal peaks caused by reflections at this ocular interface has decreased and is even weaker than the ones originating from the internal limiting membrane (peak 1 in Figure 1). In some areas the signals reflected at the retinal pigment epithelium have nearly vanished (indicated by white arrows in Figure 10). Furthermore, a thinning of the retina due to choroidal atrophy can be diagnosed and quantified when the tomogram is compared with those from the other patients investigated (Table 1).

4 CONCLUSION

The dual beam version of OCT has been used in a clinical setting for the first time and yielded cross-sectional images from normal subjects and different pathologic cases, including glaucoma, diabetic retinopathy, and different types of age-related macular degeneration. High-resolution visualization of the retinal microstructure was achieved. Therefore this instrument has potential use in ophthalmologic diagnosis, such as detection of glaucoma,¹⁷ the objective assessment of the efficiency of argon laser treatment in patients with diabetic retinopathy,¹⁸ and monitoring of AMD patients,¹⁹ as well as more

precise *in vivo* investigation of the retinal morphology of these ocular diseases. In comparing the tomograms of pathologic cases with those obtained in normal subjects, the origin of the interferometric signals detected by dual beam OCT could be investigated and elucidated, for a possible diagnostic use in ophthalmology.

Acknowledgments

The authors would like to thank Ing. H. Sattmann, Institute of Medical Physics, University of Vienna, who constructed the electronics and software of the dual beam OCT; Mr. L. Schachinger, Institute of Medical Physics, University of Vienna for technical assistance; and Dr. E. Ries and Mr. H. Semelliker from the Department of Ophthalmology of the General Hospital of Vienna for their contributions. Financial support from the Austrian Fonds zur Förderung der wissenschaftlichen Forschung (FWF Grant P 9781-MED) is acknowledged.

This paper was presented in part at the Conference on Lasers in Ophthalmology IV of the International Symposium on Biomedical Optics—BiOS Europe '96, Vienna, Austria, and at the annual meeting of the Association for Research in Vision and Ophthalmology, May 1997, Fort Lauderdale, Florida.

REFERENCES

1. G. Zinser et al., "Confocal laser tomographic scanning of the eye," *Proc. SPIE* 334-337 (1989).
2. K. Rohrschneider, R. O. W. Burk, F. E. Kruse, and H. E. Völcker, "Reproducibility of the optic nerve head topogra-

- phy with a new laser tomographic scanning device," *Ophthalmology* **101**, 1044–1049 (1994).
3. A. Tuulonen, J. Lehtola, and P. J. Airaksinen, "Nerve Fiber Layer Defects with Normal Visual Fields," *Ophthalmology* **100**, 587–597 (1993).
 4. R. N. Weinreb, A. W. Dreher, A. Coleman, H. Quigley, B. Shaw, and K. Reiter, "Histopathologic validation of Fourier-ellipsometry measurements of retinal nerve fiber layer thickness," *Arch. Ophthalmol.* **108**, 557–560 (1990).
 5. A. W. Dreher and E. D. Bailey, "Retinal nerve fiber thickness measurements by scanning laser polarimetry," in *Vision Science and Its Applications 1994*, Technical Digest Ser., Vol. 2, pp. 122–125, Optical Society of America, Washington, DC (1994).
 6. M. J. Tjon-Fo-Sang, J. De Vries, and H. G. Lemij, "Measurement by nerve fiber analyzer of retinal nerve fiber layer thickness in normal subjects and patients with ocular hypertension," *Am. J. Ophthalmol.* **122**, 220–227 (1996).
 7. M. J. Tjon-Fo-Sang and H. G. Lemij, "The sensitivity and specificity of nerve fiber layer measurements in glaucoma as determined with scanning laser polarimetry," *Am. J. Ophthalmol.* **123**, 62–69 (1997).
 8. R. C. Zeimer, M. T. Mori, and B. Khoobehi, "Feasibility test of a new method to measure retinal thickness noninvasively," *Invest. Ophthalmol. Visual Sci.* **30**, 2099–2105 (1989).
 9. R. C. Zeimer, M. Shahidi, M. Mori, S. Zou, and S. Asrani, "A new method for rapid mapping of the retinal thickness at the posterior pole," *Invest. Ophthalmol. Visual Sci.* **37**, 1994–2001 (1996).
 10. Y. S. Yang, S. Zou, R. C. Zeimer, N. M. Bressler, A. P. Schachat, and D. Finkelstein, "Quantitative mapping of the retinal thickness in diabetic eyes with clinically significant macular edema," *ARVO Abstr. Invest. Ophthalmol. Vis. Sci.* **38**, S342 (1997).
 11. A. F. Fercher, "Optical coherence tomography," *J. Biomed. Opt.* **1**(2), 157–173 (1996).
 12. D. Huang, E. A. Swanson, C. P. Lin, J. S. Schuman, W. G. Stinson, W. Chang, M. R. Hee, T. Flotte, K. Gregory, C. A. Puliafito, and J. G. Fujimoto, "Optical coherence tomography," *Science* **254**, 1178–1181 (1991).
 13. A. F. Fercher and E. Roth, "Ophthalmic laser interferometry," *Proc. SPIE* **658**, 48–51 (1986).
 14. R. C. Youngquist, S. Carr, and D. E. N. Davies, "Optical coherence domain reflectometry: a new optical evaluation technique," *Opt. Lett.* **12**, 158 (1987).
 15. K. Takada, I. Yokohama, K. Chida, and J. Noda, "New measurement system for fault location in optic waveguide devices based on an interferometric technique," *Appl. Opt.* **26**, 1603 (1987).
 16. E. A. Swanson, J. A. Izatt, M. R. Hee, F. Huang, C. P. Lin, J. S. Schuman, C. A. Puliafito, and J. G. Fujimoto, "In vivo retinal imaging by optical coherence tomography," *Opt. Lett.* **18**, 1864–1866 (1993).
 17. J. S. Schuman, M. R. Hee, C. A. Puliafito, C. Wong, T. Pedut-Kloizman, C. P. Lin, E. Hertzmark, J. A. Izatt, E. A. Swanson, and J. G. Fujimoto, "Quantification of nerve fiber layer thickness in normal and glaucomatous eyes using optical coherence tomography," *Arch. Ophthalmol.* **113**, 586–596 (1995).
 18. M. R. Hee, C. A. Puliafito, C. Wong, J. S. Duker, E. Reichel, B. Rutledge, J. S. Schuman, E. A. Swanson, and J. G. Fujimoto, "Quantitative assessment of macular edema with optical coherence tomography," *Arch. Ophthalmol.* **113**, 1019–1029 (1995).
 19. M. R. Hee, C. R. Bauman, C. A. Puliafito, J. S. Duker, E. Reichel, J. R. Wilkins, J. G. Coker, J. S. Schuman, E. A. Swanson, and J. G. Fujimoto, "Optical coherence tomography of age-related macular degeneration and choroidal neovascularization," *Ophthalmology* **103**, 1260–1270 (1996).
 20. J. G. Fujimoto, M. E. Brezinski, G. J. Tearney, S. A. Boppart, B. E. Bouma, M. R. Hee, J. F. Southern, and E. A. Swanson, "Optical biopsy and imaging using optical coherence tomography," *Nature Med.* **1**, 970–972 (1995).
 21. G. J. Tearney, M. E. Brezinski, B. E. Bouma, S. A. Boppart, C. Pitris, and J. G. Fujimoto, "In vivo endoscopic optical biopsy with optical coherence tomography," *Science* **276**, 2037–2039 (1997).
 22. C. K. Hitzenberger, "Optical measurement of the axial eye length by laser Doppler interferometry," *Invest. Ophthalmol. Vis. Sci.* **32**, 616–624 (1991).
 23. C. K. Hitzenberger, W. Drexler, C. Dolezal, F. Skorpik, M. Juchem, A. F. Fercher, and H. D. Gnad, "Measurement of the axial length of cataract eyes by laser Doppler interferometry," *Invest. Ophthalmol. Vis. Sci.* **34**, 1886–1893 (1993).
 24. W. Drexler, C. K. Hitzenberger, A. Baumgartner, O. Findl, K. Strenn, G. Rainer, R. Menapace, and A. F. Fercher, "(Sub)micrometer precision biometry of the human eye by optical coherence tomography and topography," *ARVO Abstr. Invest. Ophthalmol. Vis. Sci.* **37**, 956 (1996).
 25. W. Drexler, A. Baumgartner, O. Findl, C. K. Hitzenberger, H. Sattmann, and A. F. Fercher, "(Sub)micrometer precision biometry of the anterior segment of the human eye," *Invest. Ophthalmol. Vis. Sci.* **38**, 1304–1313 (1997).
 26. W. Drexler, A. Baumgartner, C. K. Hitzenberger, O. Findl, and A. F. Fercher, "Biometric investigation of changes in the anterior eye segment during accommodation," *Vis. Res.* **37**(19), 2789–2800 (1997).
 27. W. Drexler, C. K. Hitzenberger, H. Sattmann, and A. F. Fercher, "In vivo optical coherence tomography and topography of the fundus of the human eye," *Proc. SPIE* **2330**, 134–145 (1995).
 28. W. Drexler, C. K. Hitzenberger, H. Sattmann, and A. F. Fercher, "Measurement of the thickness of fundus layers by partial coherence tomography," *Opt. Eng.* **34**, 701–710 (1995).
 29. A. Baumgartner, B. Möller, C. K. Hitzenberger, W. Drexler, and A. F. Fercher, "Measurements of the posterior structures of the human eye in vivo by partial coherence interferometry using diffractive optics," *Proc. SPIE* **2981**, 85–91 (1997).
 30. W. Drexler, O. Findl, R. Menapace, A. Wedrich, A. Kruger, G. Rainer, A. Baumgartner, C. K. Hitzenberger, and A. F. Fercher, "Clinical feasibility of dual beam optical coherence tomography and topography for ophthalmologic diagnosis," *ARVO Abstr. Invest. Ophthalmol. Vis. Sci.* **38**, S217 (1997).
 31. M. Born and E. Wolf, "Interference and diffraction with partially coherent light," in *Principles of Optics*, pp. 491–555, Pergamon Press, Oxford (1980).
 32. W. Drexler, C. K. Hitzenberger, A. Baumgartner, O. Findl, H. Sattmann, and A. F. Fercher, "Investigation of dispersion effects in ocular media by multiple wavelength partial coherence interferometry," *Exp. Eye Res.*, in press (1997).
 33. C. K. Hitzenberger, W. Drexler, A. Baumgartner, and A. F. Fercher, "Dispersion effects in partial coherence interferometry," *Proc. SPIE* **2981**, 29–36 (1997).
 34. S. Pancharatnam, "Partial polarisation, partial coherence and their spectral description for poly-chromatic light—part II," *Proc. Ind. Acad. Sci.* **57**, 231–243 (1963).
 35. American National Standards Institute: Safe Use of Lasers, ANSI Z 136.1, American National Standards Institute, New York (1986).
 36. A. Tuulonen, J. Lehtola, and P. J. Airaksinen, "Nerve fiber layer defects with normal visual fields," *Ophthalmology* **100**, 587–597 (1993).
 37. J. Caprioli and J. M. Miller, "Videographic measurements of optic nerve topography in glaucoma," *Invest. Ophthalmol. Vis. Sci.* **29**, 1294 (1988).
 38. J. Caprioli, R. Ortiz-Colberg, J. M. Miller, and C. Tressler, "Measurements of peripapillary nerve fiber layer contour in glaucoma," *Am. J. Ophthalmol.* **108**, 404 (1989).
 39. J. Caprioli and J. M. Miller, "Measurement of relative nerve fiber layer surface height in glaucoma," *Ophthalmology* **96**, 633–639 (1989).
 40. S. J. Ryan, "Pathologic responses," and "Macular disease," in *Retina*, A. P. Schachat and R. B. Murphy, eds., Vol. 2, 2nd ed., pp. 999–1009, 1069–1103, Mosby-Year Book, Chicago (1994).